

Ab initio calculation of electron-phonon scattering time in germanium

V. G. Tyuterev and S. V. Obukhov
 Tomsk State Pedagogical University, Tomsk, Russia

N. Vast and J. Sjakste*

Ecole Polytechnique, Laboratoire des Solides Irradiés, CEA-DSM-IRAMIS, CNRS UMR 7642, 91120 Palaiseau, France
 (Received 28 March 2011; published 15 July 2011)

The intervalley scattering time in *n*-type germanium from the Γ valley to the *L*, Δ , and *X* valleys, has been computed *ab initio* with a method based on the density functional perturbation theory. We demonstrate that the pressure dependence of the lifetime of the exciton limited by the electron-phonon interaction is well described. Moreover, we discuss relaxation times measured by various pump-probe experiments at low and ambient temperatures. The contributions of the various phonons to the scattering are computed. Relaxation times due to the electron-phonon coupling are provided for each intervalley transition, as well as their behavior under pressure.

DOI: 10.1103/PhysRevB.84.035201

PACS number(s): 71.38.-k, 62.50.-p, 71.15.Mb, 71.35.-y

I. INTRODUCTION

While germanium—thought to be the most suitable material for the manufacturing of transistors at the early time of electronics—^{1,2} was supplanted by silicon, scientific interest in Ge has been renewed with the possibility of tuning the band gap in strained germanium by nanostructuring or alloying it, e.g., with silicon. In alloys, the theoretical possibility to tune the magnitude of the indirect band gap^{3,4} has proved to be particularly interesting experimentally,⁵⁻⁷ while in strained germanium nanostructures, the computed change in the band gap from indirect to direct is potentially crucial for applications in electronics or in the field of lasers.^{8,9}

These changes come from the conduction band minimum (CBM), the top of the valence band remaining at the Γ point. In fact, germanium is an indirect gap semiconductor with the lowest CBM at the *L* point (Fig. 1, left panel), but electrons close to Γ show a high mobility, due to the small effective mass (Table I, column 7). The precise knowledge of the electron-phonon scattering probability from the bottom of the Γ valley is therefore extremely important. At low pressure, only the Γ -*L* scattering is efficient, and is the dominant process in the relaxation of photoexcited carriers in intrinsic Ge.¹⁰⁻¹³ As the hydrostatic pressure increases, however, Γ - Δ and Γ -*X* scatterings come into play (center and right panels of Fig. 1), and are the main source of broadening of the excitonic linewidth,¹⁴ but their respective contributions have not been evaluated so far.

In this work, the intervalley scattering time τ has been calculated as the inverse of the electron relaxation rate γ (ERR), $\tau = \hbar\gamma^{-1}$, and the relaxation rate of an electron at the Brillouin zone (BZ) center Γ toward all of the possible final valleys *f* has been computed as a function of pressure *P*,

$$\gamma(P) = \sum_f \frac{\hbar}{2} W^f(P) \quad (1)$$

and compared with experimental data when available. The expression for the transition rate W^f has

been obtained from the application of Fermi's golden rule,¹⁵

$$W^f(P) = \frac{\pi}{MN} \sum_{\mathbf{q}\lambda} \frac{2n_{\mathbf{k}_f+\mathbf{q}}^\lambda + 1}{\omega_{\mathbf{k}_f+\mathbf{q}}^\lambda} |D_{\Gamma, \mathbf{k}_f+\mathbf{q}}^\lambda|^2 \delta(\varepsilon_\Gamma - \varepsilon_{\mathbf{k}_f+\mathbf{q}}), \quad (2)$$

where *f* stands for eight symmetry equivalent (SE) valleys *L*, six SE Δ valleys, and six SE *X* valleys. Deformation potentials $D_{\Gamma, \mathbf{k}_f+\mathbf{q}}^\lambda(P)$ for the intervalley scattering from the lowest conduction state at Γ to the final states at $\mathbf{k}_f + \mathbf{q}$ have been computed at the pressure *P* within the density functional perturbation theory (DFPT).¹⁶ As in our previous work,^{15,17} it depends on the matrix elements of the phonon-induced variation of the self-consistent Kohn-Sham potential $\Delta V_{\mathbf{k}_f+\mathbf{q}}^\lambda$:

$$D_{\Gamma, \mathbf{k}_f+\mathbf{q}}^\lambda = \sqrt{\frac{2M\omega_{\mathbf{k}_f+\mathbf{q}}^\lambda}{\hbar} |\langle \psi_\Gamma | \Delta V_{\mathbf{k}_f+\mathbf{q}}^\lambda | \psi_{\mathbf{k}_f+\mathbf{q}} \rangle|^2}. \quad (3)$$

In previous equations, *M* is the mass of the unit cell, *N* is the number of unit cells in the crystal, \mathbf{k}_f is the vector joining Γ and the minima of *L*, Δ , and *X* valleys, \mathbf{q} is the wave-vector variation around \mathbf{k}_f , $\varepsilon_{\mathbf{k}_f+\mathbf{q}}^f$ is the Kohn-Sham eigenenergy, and $\omega_{\mathbf{k}_f+\mathbf{q}}^\lambda$ and $n_{\mathbf{k}_f+\mathbf{q}}^\lambda$ are, respectively, the frequency and the Bose-Einstein occupation number of the phonon defined by the mode index λ and the wave vector $\mathbf{k}_f + \mathbf{q}$.

We have described germanium within the local-density approximation (LDA). The norm-conserving pseudopotential of Ref. 18 has been used for Ge. Kohn-Sham eigenvalues and eigenfunctions, as well as phonon frequencies and the electron-phonon matrix elements were calculated using a plane-wave basis set with a cutoff energy of 60 Ry and a Monkhorst-Pack grid of ten nonequivalent \mathbf{k} points in the irreducible BZ.

In Eq. (2), the energy conservation law in which we neglected the phonon frequency,

$$\delta(\varepsilon_\Gamma - \varepsilon_{\mathbf{k}_f+\mathbf{q}} \pm \omega_{\mathbf{k}_f+\mathbf{q}}^\lambda) \approx \delta(\varepsilon_\Gamma - \varepsilon_{\mathbf{k}_f+\mathbf{q}}), \quad (4)$$

plays an essential role as it enables us to reduce the three-dimensional integral of Eq. (2) into a search for the \mathbf{q} points on isosurfaces such that $\varepsilon_{\mathbf{k}_f+\mathbf{q}}(P) = \varepsilon_\Gamma(P)$. This is, however,

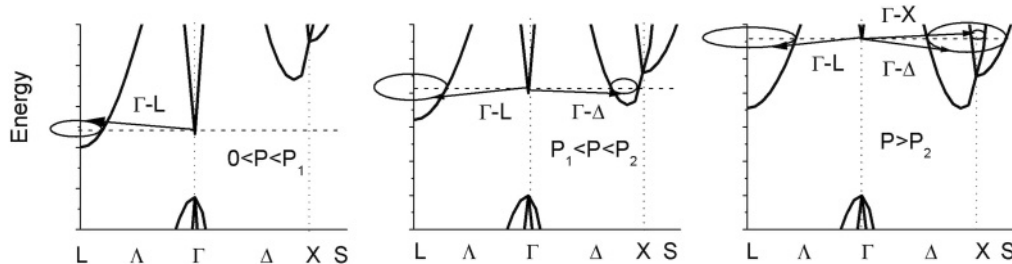


FIG. 1. Schema of electronic relaxation processes in germanium. (Left panel) Γ - L intervalley scattering for $P < 0.5$ GPa. (Center panel) Additional Γ - Δ scattering for $0.5 < P < 1.4$ GPa. (Right panel) Additional Γ - X scattering for $P > 1.4$ GPa. In the experiment, Γ - Δ and Γ - X are not distinguished (see Appendix A).

computationally heavy, and our strategy has been to first compute the energy dispersion $\varepsilon^f(P)$ of the final valleys at selected pressures with the DFT, and then design an analytical expression for each of them, as described in Appendix B. Each quadrature on the surface of constant energy $\varepsilon^f(P) = \varepsilon_\Gamma(P)$ has been performed with Gauss's formula.

II. RESULTS

The total electronic relaxation rate for the intervalley scattering from the Γ point has been computed as a function of pressure at $T = 0$ K [Fig. 2(a)]. Our results are compared with the half of the linewidth of the direct exciton in Ge, measured by optical absorption under pressure.¹⁴ Arguments in favor of the direct comparison of the calculated ERR and the excitonic linewidth have been given in our previous work.¹⁵ We compare our results to experiments up to $P = 8$ GPa, because of the structural phase transition which occurs at a pressure of 9.7 GPa, according to Refs. 19 and 14. The overall qualitative agreement between theory and experiment is remarkable as besides the shift in pressure described in Appendix A, our calculation is completely *ab initio* and does not contain any adjustable parameters.

Although in cases such as GaAs and GaP, the capacity of the DFPT to describe the electron-phonon transitions in the conduction band has already been demonstrated,¹⁵ the case of Ge was less obvious as calculations based on the DFT fail in reproducing the relative positions of the conduction band minima, in particular, when relativistic effects are taken into account²⁰ or when $3d$ states are considered as semicore states such as in Ref. 21 (Appendix A). In order to overcome this

problem, we have introduced a shift in pressure of -1.6 GPa in our pressure dependencies, and thus defined an *effective* pressure, as explained in detail in Appendix A. As one can see from Table I, the topology of the conduction band is very well described at our *effective* pressure $P = 0$. Its evolution with respect to pressure remarkably fits the experimental one [Fig. 3(a)].

The computed ERR is in extremely satisfactory agreement with the experimental halfwidth of the direct exciton [Fig. 2(a)]. At low pressure, the latter is larger than the theoretical ERR, and this is the sign that other sources of broadening can be present in the experiment. Our calculations adequately reproduce the pronounced threshold in the experimental excitonic linewidth around 0.6 GPa. According to our calculations, this threshold is due to the activation of the scattering to the Δ valley at $P_1 = 0.5$ GPa and to the X valley at $P_2 = 1.4$ GPa. This is in agreement with and adds details on the anterior interpretation of the experiments in Ref. 14. Indeed, we are able to discriminate between the contributions from the Δ and X valleys in our calculations, which has not been achieved in the experiment.

The separate contributions from the three valleys to the total ERR are shown in the panel (c) of Fig. 2, and the scattering from Γ to the X valley is responsible for as much as 20% of the linewidth at 8 GPa. Finally, at *effective* pressures larger than 2 GPa, our calculations slightly overestimate the experimental data. We attribute this discrepancy to the overestimation of the density of final states in our calculation: indeed, as shown in Fig. 3(a), the energy differences between the Γ and other valleys grow slightly faster in our calculations than in experiments, as pressure increases.

TABLE I. Relative positions of the conduction band minima (eV) and components of the effective mass tensor in units of the electron mass m_e . In this work, data have been computed at the effective pressure defined in Appendix A.

	$\Delta\varepsilon_{\Gamma L}$	$\Delta\varepsilon_{\Delta L}$	$\Delta\varepsilon_{XL}$	m_l^L	m_l^Δ	m^Γ	m_l^Δ	m_l^Δ
This work	0.11	0.19	0.38	1.56	0.07	0.05	0.89	0.19
Theory ^a	0.058	0.17	0.42	1.68	0.0816		0.91	0.19
Experiments	0.146 ^b 0.14 ^d	0.19 ^c	0.56 ^b	>1.54 ^b <1.74 ^b	<0.079 ^b <0.082 ^b			

^aFrom Table I of Ref. 22.

^bFrom Ref. 23.

^cCalled $\Delta\varepsilon_{XL}$ in Ref. 13.

^dFrom Ref. 13.

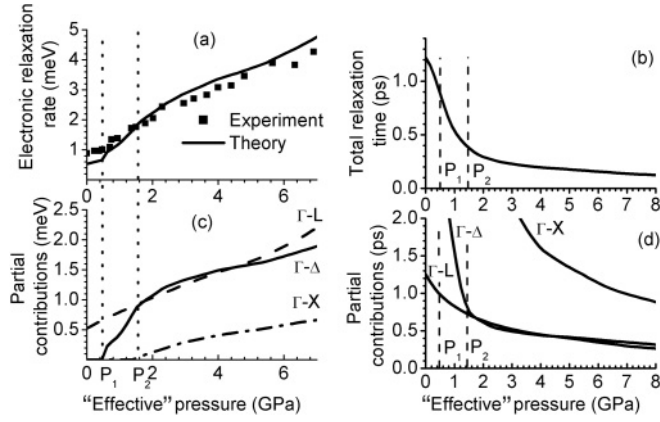


FIG. 2. Pressure dependence of the electronic relaxation rate γ [panels (a) and (c)] and of the intervalley scattering time τ [panels (b) and (d)] at low temperature. Panel (a): Total contribution of all the scattering channels to γ . (Solid line) Our calculations at $T = 0$ K. (Symbols) Excitonic halfwidth from experiment at $T = 10$ K (Ref. 14). Panel (b): Total contribution to τ . Panels (c) and (d): Partial contributions from $\Gamma \rightarrow L$, $\Gamma \rightarrow \Delta$, and $\Gamma \rightarrow X$ scattering. Pressures P_1 and P_2 are defined in the text.

The intervalley scattering time at low pressure was found to be 1.3 ps at a low temperature [Fig. 2(b)]. The lifetime that could be deduced from the experimental linewidth of the direct exciton would be much smaller. This is due to inhomogeneous broadenings present in the experiment, in particular, the one induced by the isotopic disorder.^{24,25} Therefore, our value can be considered as the theoretical intrinsic lifetime limit for electrons at Γ , and we point out the rapid decrease of the lifetime τ for pressures higher than the ambient pressure.

Our results for ERR under hydrostatic pressure can also be used to interpret pump-probe experiments, provided we make an equivalence between the experimental excitation energy and the theoretical pressure. The intervalley scattering time has been deduced from pump-probe experiments to be 0.57 ± 0.05 ps at $T = 20$ K. This transfer time to L has been determined for electrons excited at $E_{\text{exc}} = 0.1$ eV above the bottom

TABLE II. Deformation potentials D_v (eV/Å) in n -type germanium at low pressure for the virtual transitions in which the initial state is Γ and the final states are L , Δ , or X valley minima. D_v is found to be 0 for all of the transverse phonons. In the previous theoretical work of Ref. 26, $D_{\Gamma X}$ was called, respectively, $D_{\Gamma X_1}$ and $D_{\Gamma X_3}$ for LO and LA phonons.

Phonon	ω (THz)	Deformation potential (eV/Å)		
		This work	Theory ^a	Experiments
$D_{\Gamma L}$	LO	0	0	10–15 ^b , 5–6.6 ^c
	LA	4.0	3.9	4.2 \pm 0.2 ^d
$D_{\Gamma \Delta}$	LO	2.5		
	LA	5.97	0	
$D_{\Gamma X}$	LO	2.4	2.4	
	LA	2.4	2.3	

^aFrom Ref. 26.

^bFrom Ref. 27.

^cFrom Ref. 28.

^dConwell's model applied to the experiment at 300 K of Ref. 11.

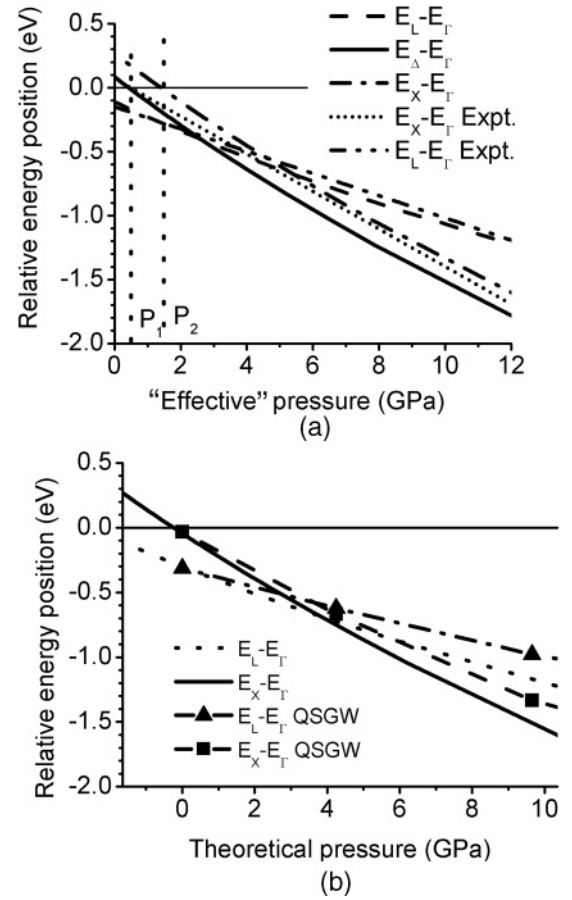


FIG. 3. Pressure dependence of the energy value of the conduction band minima with respect to the energy at Γ . Panel (a): Comparison of our computed values at L , X , and Δ with experiment Ref. 14. In the latter, the X and Δ points are not distinguished. Panel (b): Comparison of our computed values at L and X with data from the quasiparticle self-consistent GW method (Ref. 21).

of the Γ valley, by observing the decay in the luminescence signal intensity of the excited electrons.¹² In our calculations, the effective pressure for which $[\varepsilon_L - \varepsilon_\Gamma](P) = [\varepsilon_L - \varepsilon_\Gamma](P = 0) + E_{\text{exc}}$ is found to be $P \approx P_1$ [Fig. 3(a)]. At $P \approx P_1$, our calculations yield the intervalley scattering time $\tau = 0.97$ ps at $T = 10$ K, which is compatible with the experimental value of Ref. 12.

Most interestingly, the intervalley scattering time $\tau_{\Gamma \rightarrow L}$ has been attributed to the emission of LA and TA phonons,¹² because the optical deformation potential is symmetry forbidden. This is true for the virtual transitions of Table II, for which the initial electronic state is at Γ point, the final one is strictly at L point, and the energy conservation law is not fulfilled. Our values of Table II are remarkably close to the results of previous theoretical work,²⁶ and we provide additional values for the $\Gamma \rightarrow \Delta$ scattering.

When calculating the scattering time via Eqs. (2) and (3), however, the contributions of final states at $L + \mathbf{q}$ on the isosurface $\varepsilon_{L+\mathbf{q}}^f = \varepsilon_\Gamma$ are summed up, and the symmetry selection rules are lifted. It turns out that at low pressure, TA phonons do not contribute to the scattering, in contrast with the discussion of Ref. 12. This is illustrated in Fig. 4(a). In Fig. 4, we show the role of the six phonon branches in the scattering to

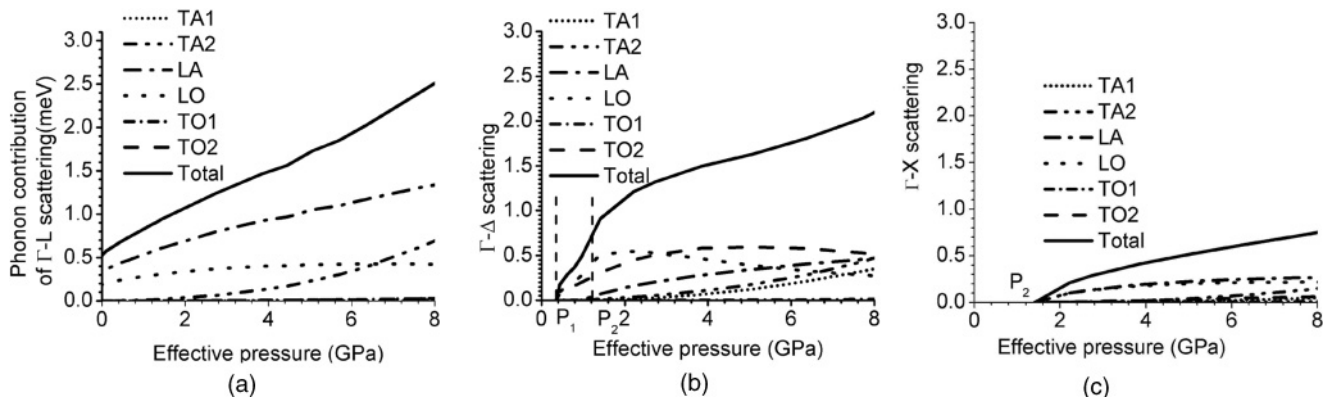


FIG. 4. Phonon contributions to the electron relaxation rate. (Left, center, and right panels) Scattering from Γ to L , Δ , and X valleys, respectively.

L , Δ , and X valleys [Figs. 4(a), 4(b), and 4(c), respectively]. For scattering to L valley, the contributions of LA and LO phonons amount, respectively, to 0.3 and 0.2 meV of the total electronic relaxation rate at ambient pressure [Fig. 4(a)].

The pressure dependences of these contributions evolve differently and result in 0.45 meV (LA) and 0.25 meV (LO) when the pressure reaches P_1 . Beyond P_1 , TO phonons start contributing in the scattering from Γ to Δ valley [Fig. 4(b)]. At pressure P_2 , considering both $\Gamma \rightarrow L$ and $\Gamma \rightarrow \Delta$ scattering, the contributions to the ERR are 0.8 meV (LO), 0.65 meV (LA), and 0.35 meV (TO). At higher pressures, the scattering from Γ to X valley becomes possible and is dominated by LO and LA phonons [Fig. 4(c)].

Finally, beyond P_2 , all of the phonons contribute to shorten the excitonic lifetime. At 8 GPa, the contribution of the two TA phonons is maximal and is only 36% of the linewidth, while scattering by LA phonons represents 40% of the ERR. One of the conclusions of this paper is that the intervalley scattering time is caused by LA and LO phonons at ambient pressure, and that most of the phonons are gradually involved in the scattering between 2 and 8 GPa, so that three-fourths of the ERR at 8 GPa is explained by LA and TA phonon scattering.

Turning to the temperature dependence of τ , our value at an ambient temperature turns out to be halved with respect to the low temperature value. At ambient pressure and temperature, the theoretical lifetime is found to be 0.54 ps, and it is 0.45 ps at $P = P_1$. In Ref. 11, the transfer time $\tau_{\Gamma \rightarrow L}$ at ambient temperature has been determined to be 0.25 ± 0.03 ps, in satisfactory compatibility with our theoretical value. More puzzling, the determination of the intervalley scattering time by subpicosecond time-resolved Raman spectroscopy yielded a relaxation time longer than ours, $\tau = 1.2 \pm 0.1$ ps at 300 K.¹⁰ In that experiment, electrons have been excited at 0.7 eV above the bottom of the conduction band at Γ and were thought to have cooled down extremely rapidly. Our theoretical value is compatible with Ref. 11, and not with Ref. 10. Our results are thus calling for a reexamination of the interpretation of the experiment of Ref. 10.

III. CONCLUSION

In conclusion, we have computed the electronic relaxation rate for the scattering from Γ to L , Δ , and X valleys by

intervalley phonons in germanium under pressure. Taking into account the dispersion of the deformation potentials in the Brillouin zone has proved to be crucial with respect to other simplified approaches. Our results based on the DFPT are in perfect agreement with the experimental linewidth of the direct exciton in that material.¹⁴ The contributions of the $\Gamma \rightarrow \Delta$ and $\Gamma \rightarrow X$ scattering channels have been separated, and the phonons responsible for the scattering have been identified. In particular, the LO phonons have been shown to yield an important contribution, as large as 40%, at low pressure and temperature, despite the fact that the optical deformation potential for virtual transitions is symmetry forbidden. The intervalley scattering time has been computed at low and ambient temperatures, and compared to data obtained by pump-probe experiments at 20 and 300 K.^{11,12}

APPENDIX A: ORDERING OF THE CONDUCTION BAND MINIMA

According to the experimental knowledge about the CBM in germanium,¹⁴ the lowest CBM is at the L point and Γ and X are, respectively, the second and third minima by order of increasing energy value. Then, at the pressure $P_1^{\text{exp}} = 0.6$ GPa,¹⁴ the latter order becomes L , X , Γ (Fig 3, upper panel, dotted, and dot-dot-dashed lines).

These subtleties in the band structure are not reproduced theoretically; the energy value is found to be lower at X than at Γ both within the DFT and the more involved QSGW method of Ref. 21, where quasiparticle corrections are taken into account self-consistently [Fig. 3(b), symbols]. In the QSGW calculation, the $3d$ states have been included in the valence. This turns out to yield a rather bad description of the relative positions of the CBM $\varepsilon_L - \varepsilon_\Gamma$ and $\varepsilon_X - \varepsilon_\Gamma$ with respect to the experiment (Fig. 3). In the present work, $3d$ states have been kept frozen in the core. The volume has been slightly expanded with respect to the theoretical one to counterbalance the overbinding coming from our use of the LDA. At low pressure, this amounts to work at the experimental lattice parameter $a = 5.66$ Å instead of the theoretical equilibrium $a = 5.62$ Å, with the effective pressure $P = -1.6$ GPa. At other pressures, we have maintained this pressure shift of -1.6 GPa constant up to 8 GPa.

Under this condition, the computed values of the relative energy of the CBM and the components of the effective mass tensor are in satisfactory agreement with experimental ones (Table I), and differences with the theoretical data of Ref. 22 are small.

At higher pressures, the transition from $L < \Gamma < X$ to $L < X < \Gamma$ is recovered at the effective pressure of $P_1 = 0.5$ GPa, very close to the experimental value $P_1^{\text{exp}} = 0.6$ GPa. Moreover, the experimental and computed pressure dependencies of $\varepsilon_L - \varepsilon_\Gamma$ are quasi-identical up to 8 GPa [Fig. 3(a), dashed and dot-dot-dashed line].

Experimentally, the CBM at X has not been distinguished from the minimum at Δ . In our calculations, the X scattering channel is active only for $P > P_2$ with $P_2 = 1.4$ GPa. The pressure dependence of $\varepsilon_X - \varepsilon_\Gamma$ (dotted line) observed experimentally is close to the theoretical $\varepsilon_\Delta - \varepsilon_\Gamma$ at low pressure (solid line), and to the $\varepsilon_X - \varepsilon_\Gamma$ at high pressure (dot-dashed line). This is experimental proof that the distinction between the CBM at X and at Δ holds, and is not an artifact of the calculations.

To summarize, the pressure ordering of the CBM is the following one (Fig. 1): (i) $L < \Gamma < \Delta < X$ for $P < P_1$; (ii) $L < \Delta < \Gamma < X$ for $P_1 < P < P_2$; (iii) $L < \Delta < X < \Gamma$ for $P_2 < P$.

APPENDIX B: ANALYTICAL EXPRESSION FOR THE ENERGY DISPERSION

In this work, the energy dispersion of the L , Δ , and X valleys of the conduction band was studied at different effective pressures between 0 and 8 GPa, within DFT. It has been then approximated by an analytical function, fitted on the DFT results.

The energy dispersion of the lowest conduction band around the L point turned out to be nonparabolic on the whole pressure range. It has been approximated by defining a system of cartesian coordinates (ξ, η, λ) whose origin was at L , such that

$$\varepsilon_{L+\mathbf{q}}^f = \varepsilon_L + \frac{\hbar^2(q_\eta^2 + q_\xi^2)}{2m_t} \left(1 - \alpha \frac{\hbar^2(q_\eta^2 + q_\xi^2)}{2m_t} \right) + \frac{\hbar^2 q_\lambda^2}{2m_l}, \quad (\text{B1})$$

where the parameter α accounts for the nonparabolicity of the dispersion, m_l and m_t are the components of the effective mass tensor at L , the λ axis is directed along Λ , and the axes η and ξ lie in the hexagonal edge plane of the BZ (Fig. 5). The fit parameters m_l , m_t , and α turned out to be linearly dependent on the pressure, with values ranging, respectively, from $1.56 m_e$, $0.073 m_e$ (Table I), and 0.52 eV^{-1} at low pressure, to the values $1.67 m_e$, $0.093 m_e$, and 0.24 eV^{-1} at an effective pressure of 8 GPa. The shape of the isosurface describing the final states available for the intervalley scattering to L valley, $\varepsilon_{L+\mathbf{q}}^f(P) = \varepsilon_\Gamma(P)$, is shown in Fig. 6(a).

The Δ valley minimum of the first conduction band is found at six positions, symmetry equivalent to the BZ point $(0, 0, \frac{2\pi}{a(P)} - q_0)$, with $q_0 = 0.185$ and 0.177 in units $2\pi/a(P)$, and $a = 5.66$ and 5.44 \AA at 0 and 8 GPa, respectively. Very close to the Δ valley minimum, the energy dispersion

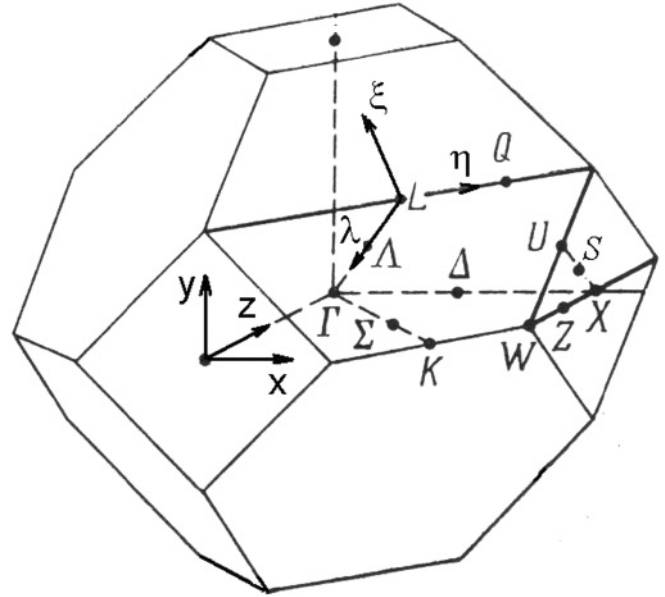


FIG. 5. Definition of systems of coordinates in the reciprocal space used for the analytical expressions of the energy dispersion (Appendix B).

of the first conduction band is parabolic. At pressures beyond P_2 , the second conduction band dispersion is needed (X valley scattering) as well as that of the first one (Δ scattering).

The analytical formulation of the first and second conduction band dispersion around the X point has been made with the help of the components of the effective mass tensor m_l and m_t . The latter turned out to depend linearly on pressure, and were equal to 0.89 and $0.19 m_e$ at low pressure (Table I), and to 0.92 and $0.22 m_e$ at 8 GPa. For the \mathbf{q} point, the cartesian coordinate system of Fig. 5 has been used. Its origin is at the point X , and z axis is directed from X to Γ along one selected Δ direction, while x and y axes are directed along two equivalent directions in the square edge plane of the BZ, yielding

$$\varepsilon_{X+\mathbf{q}}^{f,1/2} = \varepsilon_X + \frac{\hbar^2(q_x^2 + q_y^2)}{2m_t} + \frac{\hbar^2(q_z^2 + q_0^2)}{2m_l} \pm \hbar^2 \sqrt{\sigma^2 \frac{q_x^2 q_y^2}{m_t^2} + \frac{q_z^2 q_0^2}{m_l^2}}, \quad (\text{B2})$$

where the index 1 (respectively, 2) is related to the first (respectively, second) conduction band, and to the + (respectively, -) sign in the last term in Eq. (B2). The fit parameter σ represents the nonparabolicity of the band far from the Δ CBM, it turned out to be linearly dependent on pressure, ranging from the value 0.843 at low pressure, to the value 0.832 at 8 GPa. At the X point, first and second conduction bands are degenerate.

The isosurface $\varepsilon_{X+\mathbf{q}}^{f,1}(P) = \varepsilon_\Gamma(P)$ is shown in Fig. 6(b) for the pressures $P_1 < P < P_2$. Its shape is quasiellipsoidal. Interestingly, at pressures $P_2 < P$, this isosurface shows a pronounced goffered shape [Fig. 6(c)]. Moreover, at these pressures, another constant energy surface $\varepsilon_{X+\mathbf{q}}^{f,2}(P) =$

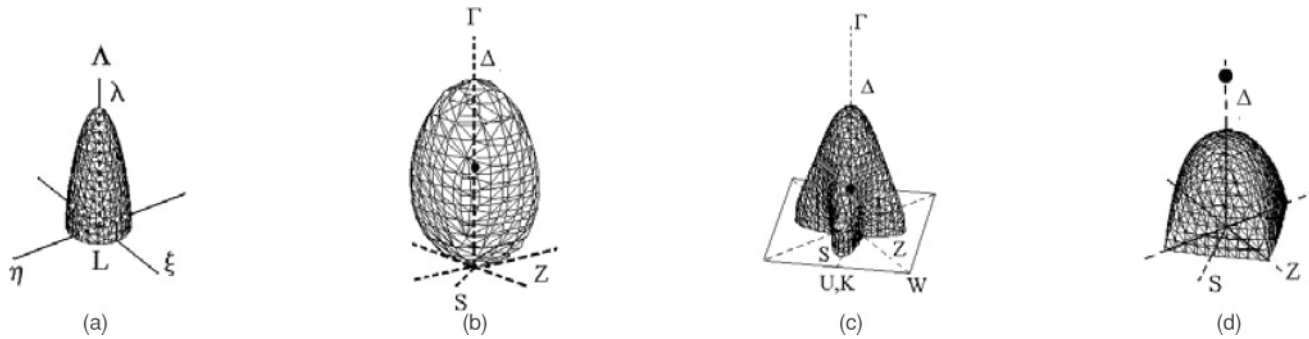


FIG. 6. Constant energy surfaces for L , Δ , and X valleys available for the intervalley scattering from Γ at various pressures. Note that, in panels (b), (c), and (d), the scaling is different: the bold circle indicates the position of the Δ valley minimum.

$\varepsilon_{\Gamma}(P)$ is inserted inside the gofferred-shaped surface [Fig. 6(d)].

To summarize, the isosurface for $P < P_1$ consists of one sheet per L valley, with $\varepsilon_{L+q}^f(P) = \varepsilon_{\Gamma}(P)$, where $\varepsilon_{L+q}^f(P)$ is modeled by Eq. (B1) [Fig. 6(a)]. One additional isosurface per Δ valley, comes into play when $P_1 < P < P_2$, defined by $\varepsilon_{X+q}^{f,1}(P) = \varepsilon_{\Gamma}(P)$, where $\varepsilon_{X+q}^{f,1}(P)$ is modeled by Eq. (B2). At those pressures, the isosurface is quasiellipsoidal [Fig. 6(b)]. At higher pressures, $P_2 < P$, the isosurface $\varepsilon_{X+q}^{f,1}(P)$ becomes gofferred, and encloses an additional isosurface, $\varepsilon_{X+q}^{f,2}(P) = \varepsilon_{\Gamma}(P)$, where $\varepsilon_{X+q}^{f,2}(P)$ is modeled by Eq. (B2) [Figs. 6(c) and 6(d)]. Finally, each quadrature on above-described

surfaces of constant energy has been performed with Gauss's formula.

ACKNOWLEDGMENTS

This work has been supported by the Russian Science and Innovations Federal Agency under Contract No. 02.740.11.0238, Rosobrasovanie Grant No. 01.2.007 01695 and French ANR (Project PNANO ACCATTONE). Results have been obtained with the Quantum Espresso package (Ref. 16). We acknowledge support from the DGA. Computer time has been granted by IRSC SKIF of Tomsk State University, CEA/DSM (project p93) and GENCI (project 2210).

*jelena.sjakste@polytechnique.edu

¹L. Krugman, *Fundamentals of Transistors* (Chapman and Hall Ltd., London, 1954).

²M. Riordan, in *Silicon Materials Science and Technology: Proceedings of the Eighth International Symposium on Silicon Materials Science and Technology*, edited by H. R. Huff, U. Gösele, and H. Tsuya (The Electrochemical Society, Pennington, NJ, 1998), Vol. 1, pp. 134–138.

³M. M. Rieger and P. Vogl, *Phys. Rev. B* **48**, 14276 (1993).

⁴M. Rieger and P. Vogl, *Phys. Rev. B* **50**, 8138 (1994).

⁵G. Abstreiter, *Phys. Scr.*, **T 49**, 42 (1993).

⁶D. Paul, *Semicond. Sci. Technol.* **19**, R75 (2004).

⁷D. Paul, *Oxford Handbook of Nanoscience and Technology*, edited by A. V. Navliker and Y. Y. Fu (Oxford University Press, Oxford 2010).

⁸P. Vogl, M. Rieger, J. Maewski, and G. Abstreiter, *Phys. Scr.*, **T 49**, 476 (1993).

⁹F. Zhang, V. H. Crespi, and P. Zhang, *Phys. Rev. Lett.* **102**, 156401 (2009).

¹⁰K. Tanaka, H. Ohtake, and T. Suemoto, *Phys. Rev. Lett.* **71**, 1935 (1993).

¹¹X. Q. Zhou, H. M. van Driel, and G. Mak, *Phys. Rev. B* **50**, 5226 (1994).

¹²G. Mak and W. W. Rühle, *Phys. Rev. B* **52**, R11584 (1995).

¹³J. Hebling, M. C. Hoffmann, H. Y. Hwang, K.-L. Yeh, and K. A. Nelson, *Phys. Rev. B* **81**, 035201 (2010).

¹⁴G. H. Li, A. R. Goñi, K. Syassen, and M. Cardona, *Phys. Rev. B* **49**, 8017 (1994).

¹⁵J. Sjakste, N. Vast, and V. Tyuterev, *Phys. Rev. Lett.* **99**, 236405 (2007).

¹⁶S. Baroni, S. de Gironcoli, A. Dal Corso, and P. Giannozzi, *Rev. Mod. Phys.* **73**, 515 (2001).

¹⁷J. Sjakste, V. Tyuterev, and N. Vast, *Phys. Rev. B* **74**, 235216 (2006).

¹⁸X. Gonze, R. Stumpf, and M. Scheffler, *Phys. Rev. B* **44**, 8503 (1991).

¹⁹S. Klotz, J. M. Besson, M. Braden, K. Karch, P. Pavone, D. Strauch, and W. G. Marshall, *Phys. Rev. Lett.* **79**, 1313 (1997).

²⁰G. B. Bachelet and N. E. Christensen, *Phys. Rev. B* **31**, 879 (1985).

²¹P. Modak, A. Svane, N. E. Christensen, T. Kotani, and M. van Schilfgaarde, *Phys. Rev. B* **79**, 153203 (2009).

²²F. Murphy-Armando and S. Fahy, *Phys. Rev. B* **78**, 035202 (2008).

²³*Landolt-Börnstein, Semiconductors: Physics of Group IV Elements and III–V Compounds*, edited by O. Madelung, H. Weiss, and M. Schulz (Springer-Verlag, Berlin, 1982), Vol. 17a.

²⁴V. Tyuterev, J. Sjakste, and N. Vast, *Phys. Rev. B* **81**, 245212 (2010).

²⁵N. Vast and S. Baroni, *Phys. Rev. B* **61**, 9387 (2000).

²⁶S. Krishnamurthy and M. Cardona, *J. Appl. Phys.* **74**, 2117 (1993).

²⁷D. Chattopadhyay and B. Nag, *Phys. Rev. B* **4**, 1220 (1971).

²⁸D. Chattopadhyay, *Phys. Rev. B* **7**, 4739 (1973).